Eng. Sci., 2025, **35**, 1578

Engineered Science
DOI: https://dx.doi.org/10.30919/es1578

Hydrophobic β-Carotene Passivation toward Efficient and Stable Perovskite Solar Cells

Haogang Meng, Xiaohui Li, Youfang Zheng, Congmin Hou, Yongxiang Mai, Meiyue Liu, Zeng Chen, Putao Zhang* and Shengjun Li*

Abstract

Perovskite, as a synthetic functional material, has garnered significant research attention in recent years due to its exceptional optoelectronic properties and cost-effectiveness in photovoltaic applications. However, one of the most prominent challenges in practical applications remains the inadequate environmental stability of perovskite materials. This study aims to identify a natural, low-cost additive that can simultaneously enhance operational stability and passivate internal crystal defects, thereby improving photoelectric conversion efficiency. We successfully achieved this objective by utilizing β-carotene molecule. As a highly abundant and stable natural pigment, it offers notable cost advantages, exhibiting potent antioxidant effects and regulate perovskite energy level. Incorporation studies of β-carotene in tri-cation perovskite systems demonstrate its efficacy as a long-chain passivator, reducing crystalline defects and enhancing grain compactness. Current-voltage measurements reveal that β-carotene incorporation boosts the champion power conversion efficiency (PCE) of (CsFAMA)Pb(I/Br)$_3$ perovskite solar cells from 20.49% to 23.38%, corresponding to a 14.1% relative enhancement. Moreover, its excellent antioxidant and moisture resistance properties ensure that the PCE remains above 89% of the initial value after exposure to environmental humidity for 500 hours. We report a natural pigment-based molecular modulator that concurrently addresses defect passivation and environmental protection, achieving simultaneously enhanced PCE and stability in high-performance perovskite photovoltaics.

Keywords: Perovskite solar cells; Efficiency; Stability; Antisolvent post-treatment; β-Carotene.
Received: 28 March 2025; Revised: 13 April 2025; Accepted: 14 April 2025.
Article type: Research article.

1. Introduction

Perovskite solar cells (PSCs) exhibit a theoretical efficiency limit substantially surpassing that of conventional silicon-based photovoltaic cells, with their power conversion efficiency (PCE) demonstrating remarkable progress in recent years.[1-3] The latest research indicates that the photoelectric conversion efficiency of single-junction perovskite solar cells has surpassed 26.4%.[4] Perovskite materials are abundant in raw materials, easy to synthesize, and cost-effective, attracting considerable attention from researchers. However, for commercialization, perovskite devices still face numerous challenges.[5-7]

Perovskite materials belong to ionic crystals, which makes their structure susceptible to water solubility. Specifically, formamidine lead iodide (α-FAPbI$_3$), a key component of the black-phase perovskite, readily deliquesces at room temperature, transforming into the wide-bandgap yellow-phase formamidine lead iodide (δ-FAPbI$_3$).[8-10] This sensitivity to environmental factors such as moisture and oxygen results in poor long-term operational stability of the devices. Additionally, organic-inorganic hybrid perovskite materials are prone to ion migration under light and high-temperature conditions, leading to defect accumulation and impurity formation.[11-13] This not only damages the film's morphology but also alters its electrical properties, thereby reducing photoelectric conversion efficiency. Furthermore, crystal phase defects trap charge carriers, forming positive and negative charge centers that cause non-radiative recombination and accelerate device degradation.[14,15] Grain boundary defects, which are more prevalent than those within the crystal, are another major source of non-radiative recombination.[16] Identifying suitable additives to passivate

Henan Key Lab Quantum Materials & Quantum Energy, School of Future Technology, Henan University, Henan, Kaifeng, 475001, China
**E-mail*: putaozhang@henu.edu.cn (P. Zhang); lishengjun@henu.edu.cn (S. Li)

grain boundaries remains a critical challenge.

The tricationic perovskite system allows for adjustable bandgaps through the doping of different elemental components. Substituting FA^+ ions with a small number of Cs^+ ions can induce volume shrinkage of the perovskite cubic octahedron, enhancing the binding force between FA^+ and iodide ions.[17,18] Multi-cationic perovskite materials have been shown to improve the purity of the perovskite crystal phase, thereby enhancing both photoelectric conversion efficiency and environmental stability. However, the heterogeneous radius of various ions leads to multifaceted grain growth, resulting in high-density potential defects and significant non-radiative recombination. Studies have demonstrated that long alkyl chain compounds can inhibit perovskite nucleation.[19] The presence of hydrogen bonds in these additives helps suppress the complex mesophase of perovskites, promoting directed growth of α-$FAPbI_3$ in multi-cationic organic-inorganic hybrid perovskites. Long alkyl chains can attach to perovskite crystal nuclei via strong van der Waals interactions, forcing closer contact between perovskite crystals.[20] According to Ostwald ripening theory, well-oriented grain growth consumes adjacent randomly oriented grains. The presence of alkyl chains may effectively assist in achieving isotropy in perovskite grains, leading to higher crystallinity, efficiency, and moisture stability. The introduction of macromolecular chains also inhibits the formation of α-phase perovskite crystals, allowing low-shape nuclei with advantageous adhesion surfaces to grow into larger grains.[21]

Therefore, we investigated the introduction of carotenoid additives at both the inner grain boundaries and the upper crystal interfaces of perovskite crystals. This approach aimed to optimize crystal growth conditions and minimize internal crystal defects. β-Carotene, a naturally abundant and stable pigment, possesses an extended polyene backbone with numerous π-π conjugated double bonds.[22] Additionally, β-carotene exhibits potent antioxidant effects, as documented in literature.[23,24] Oxygen can oxidize lead ions in perovskite films to PbO_2, accelerating structural degradation. β-carotene effectively protects Pb^{2+} ions from forming superoxide O^{2-} ions under light exposure, thereby significantly extending the operational lifespan of unpackaged perovskite devices in conventional environments.[25] The numerous -CH bonds in β-carotene molecules and the abundance of benzene rings in the spiro-OMeTAD layer facilitate spontaneous CH-π stacking, constructing efficient charge transport channels that enhance carrier separation and extraction.[26] Moreover, the conjugated double bonds in β-carotene can bond with uncoordinated Pb^{2+} ions at the perovskite crystal interface, effectively passivating defects.[27] Our results demonstrate that the $Cs_{0.05}(FA_{0.93}MA_{0.07})_{0.95}Pb(I_{0.95}Br_{0.04}Cl_{0.01})_3$ perovskite positive device, treated with single anti-solvent doping, achieved an efficient and stable device structure. Device efficiency increased from 20.89% to 23.38%, maintaining efficient operation for more than 500 hours at conventional air humidity.

2. Experimental

2.1. Material selection

1mm thick resistance 15 Ω indium tin oxide (ITO) conductive glass substrate purchased from Juntai solar photovoltaic technology, Tin oxide colloidal dispersion (Tin (IV) Oxide, 12 wt% in H_2O colloidal dispersion), DMF (99.9%) purchased from Aladdin, DMSO(99.9%) is purchased from Primacy Technologies, PbI_2 (99.999%) ,Ultra dry chlorobenzene (99.95%), MABr (99.8%), FAI (99.8%), MACl (99.8%), $PbBr_2$ (99.8%), IPA (99.9%) , 4-tBP (98%), Spiro-OMeTAD (99.8%), Li-TFSI (99.95%) , An analytical grade standard of β-carotene purchased at Aladdin.

2.2. Device fabrication

After ultrasonic cleaning of 1.1 mm thick indium tin oxide (ITO) conductive glass with a sheet resistance of 15 Ω using a dedicated cleaning solution, the substrate was dried in an oven. The cleaned ITO substrate was then spin-coated with a 12 wt% SnO_2 dispersion at 3000 rpm for 30 seconds and subsequently annealed at 150 °C for 20 minutes. In a nitrogen-filled glovebox, 80 μL of a 1.2 M tricationic perovskite precursor solution was deposited onto the electron transport layer by spin coating at 1000 rpm for 10 seconds, followed by accelerating to 4000 rpm for 30 seconds. During this process, 120 μL of anti-solvent chlorobenzene (CB) was added dropwise over 10 seconds. The coated film was annealed at 100 °C for one hour. For experimental devices, 0.05 mM β-carotene was doped into the anti-solvent chlorobenzene (CB), while 1 mM β-carotene was spin-coated onto the annealed perovskite surface. A spiro-OMeTAD hole transport layer was formed by spin coating at 4000 rpm for 30 seconds and oxidized in a desiccator for 12 hours. Finally, a 120 nm silver electrode was evaporated to complete the perovskite solar cell device.

2.3. Characterizations

Photocurrent-voltage curves were obtained under one standard simulated sunlight (AM1.5, 100 mW cm^{-2}) using a source meter (Keithley 2400). Before the test, calibrate the light intensity with Si standard cell. The effective area of the cells were defined to be 0.04cm2. The Incident photon-to-current efficiency (IPCE) was conducted on an IPCE test system (500ADX, USA). The surface morphology of perovskite films was characterized by JEOL JSM-7610F Plus field emission scanning electron microscopy system. The perovskite crystal arrangement was analyzed by JEOL JEM-F2000 200KV field emission transmission electron microscope. The phase transformation of perovskite minerals was observed with the X-ray powder diffractometer Bruker D8 Advance produced by Bruker GMBH. The surface flatness and surface potential distribution of perovskite were observed with MFP-3D Origin+ scanning probe microscope produced by Oxford Instruments, USA. The obtained signal was tested by FLS1000 time-resolved variable-temperature fluorescence spectrometer. The UV-VIS absorption signal was measured by

UH4150 UV-VIS near infrared spectrophotometer. The impedance signal is obtained by testing with electrochemical workstation (Zahner, IM6).

3. Results and discussion

In the perovskite system primarily composed of $FAPbI_3$, doping with a small amount of Cs^+ and MA^+ is believed to facilitate reduced photovoltaic hysteresis. Additionally, this approach can mitigate the ion migration effect induced by light-enhanced polarization. However, this system exhibits a higher density of defects at grain boundaries, leading to carrier trapping and consequent reduction in photocurrent. This also affects the decay time of photoluminescence. Moreover, under standard humidity and temperature conditions, the stability of these perovskite films is compromised, with stress-induced defects widely distributed within the crystal lattice and at grain boundaries. To address these issues, we introduced naturally stable β-Carotene into the CB antisolvent system. It is anticipated that β-Carotene will serve as both a perovskite grain growth inhibitor and a crystal interface passivator, while simultaneously enhancing carrier transport channels with the spiro-OMeTAD interface. Fig. 1a illustrates the molecular structure of β-Carotene. As a natural long-chain hydrocarbon, β-Carotene contains numerous -CH bonds that tend to form CH-π conjugations with benzene rings, thereby facilitating efficient charge transport pathways. The extensive C=C double bonds promote chemical crosslinking, which aids in suppressing ion migration and defect passivation. Furthermore, as a hydrophobic organic macromolecule, β-Carotene effectively prevents water and oxygen from infiltrating the perovskite lattice, thus inhibiting the degradation of the black phase (α-$FAPbI_3$). Fig. 1b outlines the primary steps involved in spin-coating perovskite layers. Fig. 1c compares the nucleation and growth diagrams of perovskite grains before and after the addition of β-Carotene to the antisolvent. The introduction of β-Carotene significantly inhibits perovskite nucleation. Due to strong van der Waals interactions between adjacent alkyl chains, β-Carotene tends to adhere to perovskite nuclei, promoting tighter contact between perovskite crystals and resulting in grains with superior crystallization and more uniform orientation.

In order to explore the mechanism of action of β-Carotene on perovskite solar cells, we have tried several ways. It was added into the anti-solvent CB for doping treatment (β-carotene for short), it is dissolved in CB as a perovskite surface passivation agent (Treat for short), and it is added to the perovskite precursor solution. Adding β-carotene to the perovskite precursor solution did not significantly enhance the photovoltaic conversion efficiency of the final device (Fig. S1). Fig. 2a illustrates the UV-Vis absorption spectra before and after treatment. The results show that the light absorption signal of perovskite films with β-carotene added in different ways is gradually enhanced, and the inflection point of curve decline is slightly shifted. Fitting results combined with Fig. 2b show that the treatment had minimal influence on the band gap of perovskite. To gain deeper insights into the role of β-Carotene in perovskite films, we conducted X-ray Photoelectron Spectroscopy (XPS) characterization. As shown in Figs. 2c and d, Pb 4f and I 3d peaks in the perovskite filmtreated with β-Carotene exhibited higher binding energies

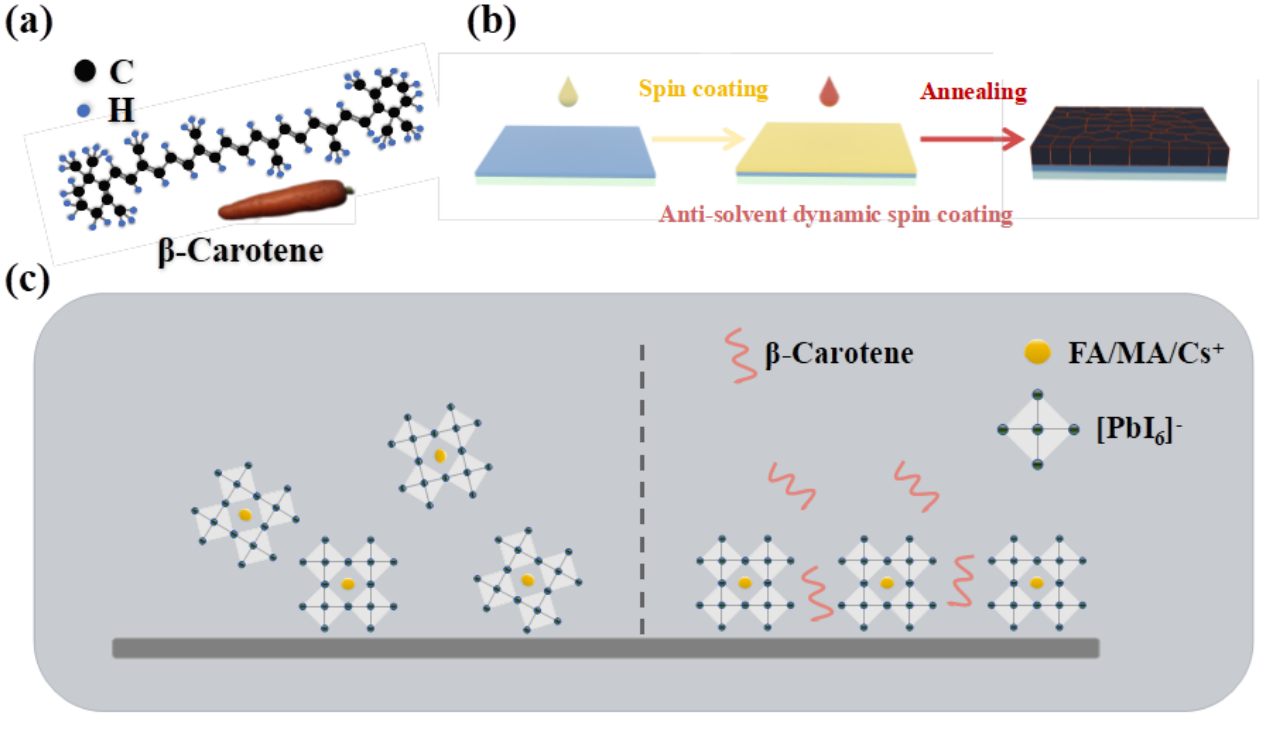

Fig. 1: (a) Molecular structure of β-Carotene. (b) Schematic diagram of spin-coating process. (c) Schematic diagram of perovskite grain nucleation before and after adding β-carotene to antisolvent CB.

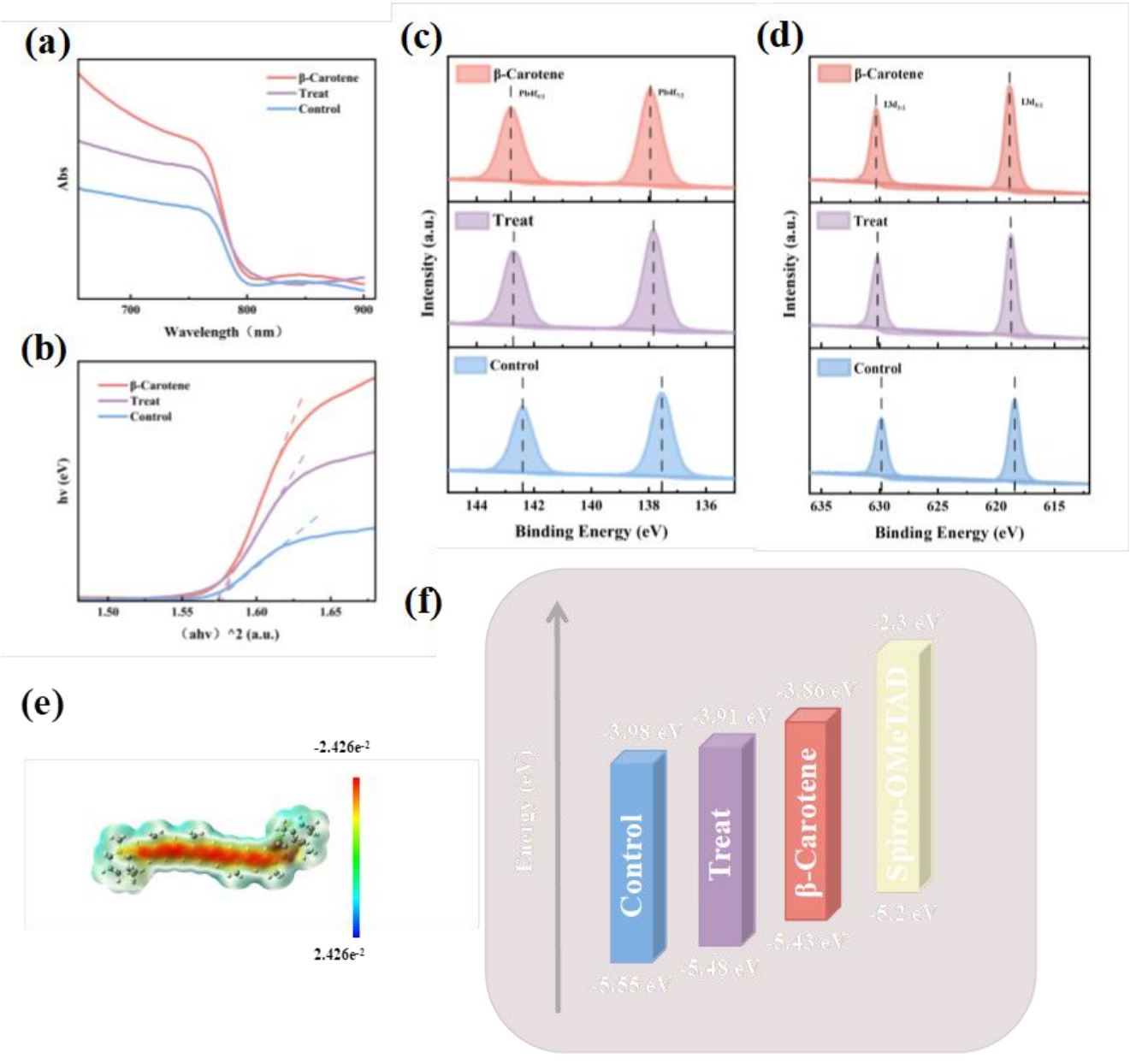

Fig. 2: (a) UV-Vis absorption test diagram of control group, passivation treatment group and anti-solvent addition group. (b) Schematic diagram of perovskite band gap distribution after fitting the UV-Vis absorption test results. (c) XPS spectra of Pb 4f and (d) I 3d perovskite films. (e) ESP distribution of β-Carotene. (f) The energy level distribution diagram of perovskite before and after treatment is drawn by calculating the Ev of perovskite through ultraviolet photoelectron spectroscopy (UPS).

compared to the control film. This suggests that the rapid nucleation of the precursor solution after spin-coating was inhibited post-treatment. Additionally, the higher binding energy indicates a more stable crystal structure, which helps suppress lead ion migration. The long-chain structure with peripheral electron deficiency leads to stronger hydrogen bonding, further explaining the increased $[PbI_6]^-$ binding energy and more stable perovskite crystal structure.[27] The HOMO and LUMO orbitals of β-Carotene molecules are shown in Fig. S2. The electrostatic potential (ESP) of β-carotene molecules is shown in Fig. 2e. It can be observed that a large number of conjugate double bonds in the molecular skeleton have a high electron cloud density, which leads to an increase in CBM on the upper surface of perovskite. Fig. 2f shows that the bottom energy level of perovskite conduction band gradually increases from -3.98 to -3.86 eV, facilitating easier carrier transition in the treated perovskite film. Moreover, the upward bending of the energy level better matches the hole transport layer Spiro-OMeTAD, potentially leading to higher Voc.[28,29] The inhibition of rapid disordered nucleation in the tricationic perovskite system and the adjustment of energy level alignment between the perovskite layer and the hole transport layer highlight the significant value of adding β-Carotene.

We further investigated the crystallinity of perovskite crystals. The X-ray diffraction (XRD) results presented in Fig.

3a indicate that compared to unmodified perovskite thin films, post-treatment passivation with β-Carotene on the surface of perovskite did not significantly alter its overall crystallinity. However, the diffraction signal intensity for the (100) and (200) crystal planes of perovskite was notably enhanced after antisolvent doping treatment (highlighted by the light brown background area). Conversely, the intensity of the (110) and (111) crystal planes within this region was suppressed and did not increase proportionally with the main peak intensity, particularly that of the (200) plane. This suggests that the incorporation of β-Carotene molecular chains effectively promoted grain growth while inhibiting the formation of inferior crystal surfaces, thereby providing a more orderly nucleation environment for perovskite grains. Notably, the addition of β-Carotene led to the near disappearance of the PbI_2 characteristic peak, indicating a reduction in crystal defects and an enhancement in device stability. The scanning electron microscope images in Figs. 3b and c visually demonstrate the morphological changes in perovskite grains following β-Carotene processing. The grain size increased substantially (Fig. 3d), while the residual lead iodide in the labeled areas decreased significantly. It is noteworthy that when the doping concentration of β-Carotene in the antisolvent was increased to 1 mM, the grain size of the perovskite crystals observed under scanning electron microscopy (SEM) significantly increased, and the lead iodide on the surface nearly vanished. However, this also led to evident grain collapse (Fig. S3) and a rapid decline in device efficiency (Fig. S4). This suggests that an excessive amount of nearly insulating organic material within the perovskite lattice disrupts the carrier transport channels, and the advantages conferred by denser crystal growth are insufficient to offset these adverse effects. The atomic force microscopy (AFM) image in Fig. 3e shows that after doping β-Carotene into the antisolvent, the grain roughness at the perovskite interface decreased from 20.40 to 15.56 nm post-annealing, suggesting fewer defect states and potentially higher Voc values. The observed variation in grain size is consistent with the SEM results. The increased surface potential of perovskite facilitates hole extraction and reduces charge recombination, signaling improved device performance and stability (Figs. 3g and h).

To elucidate the impact of β-Carotene-doped antisolvent on the carrier recombination process within perovskite crystals, we conducted photoluminescence (PL) tests on perovskite thin films. As illustrated in Fig. 4a, the incorporation of β-Carotene molecular chains markedly enhanced the PL signal of the original perovskite film. Additionally, a slight redshift was observed at the signal peak, indicating an increased absorption of longer wavelength light. This broader light absorption range

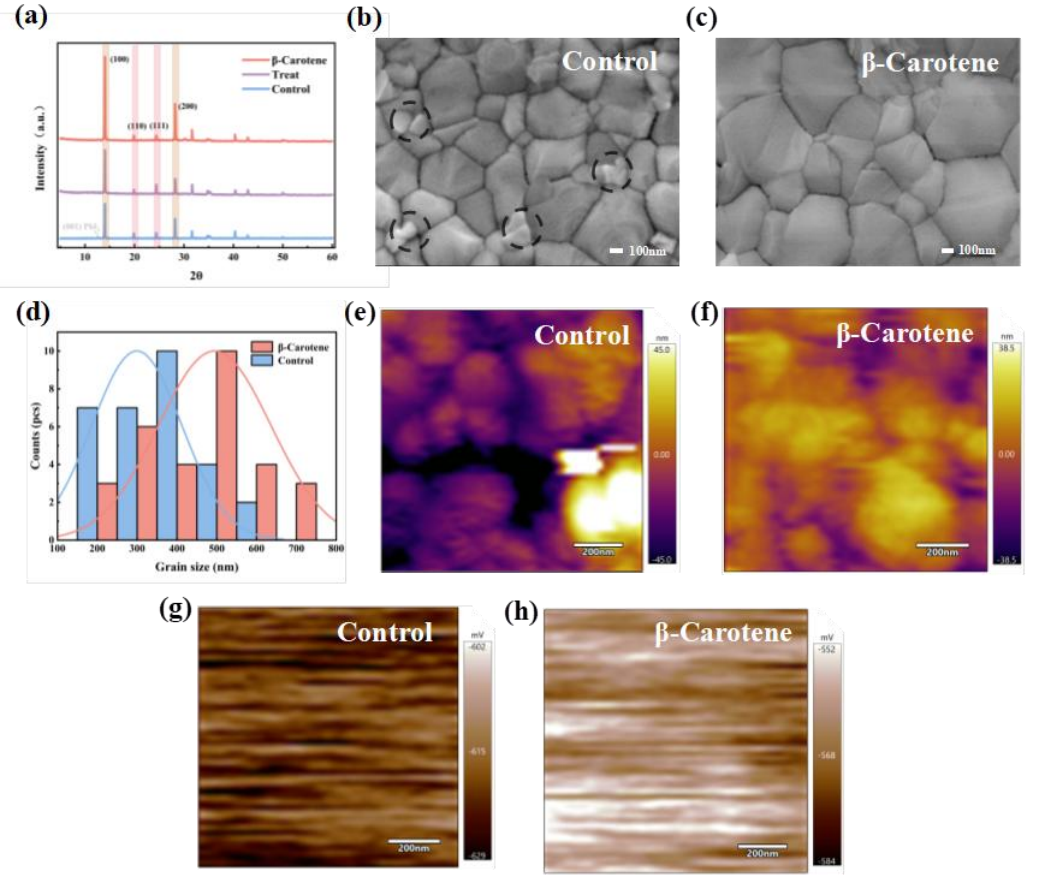

Fig. 3: (a) XRD images of control group, surface passivation treatment group and β-Carotene group. (b, c) SEM images of perovskite grains before and after β-Carotene was added to the antisolvent. (d) perovskite particle size distribution map. (e, f) AFM test diagram. (g, h) kelvin probe force microscopy (KPFM) test results, perovskite surface potential diagram.

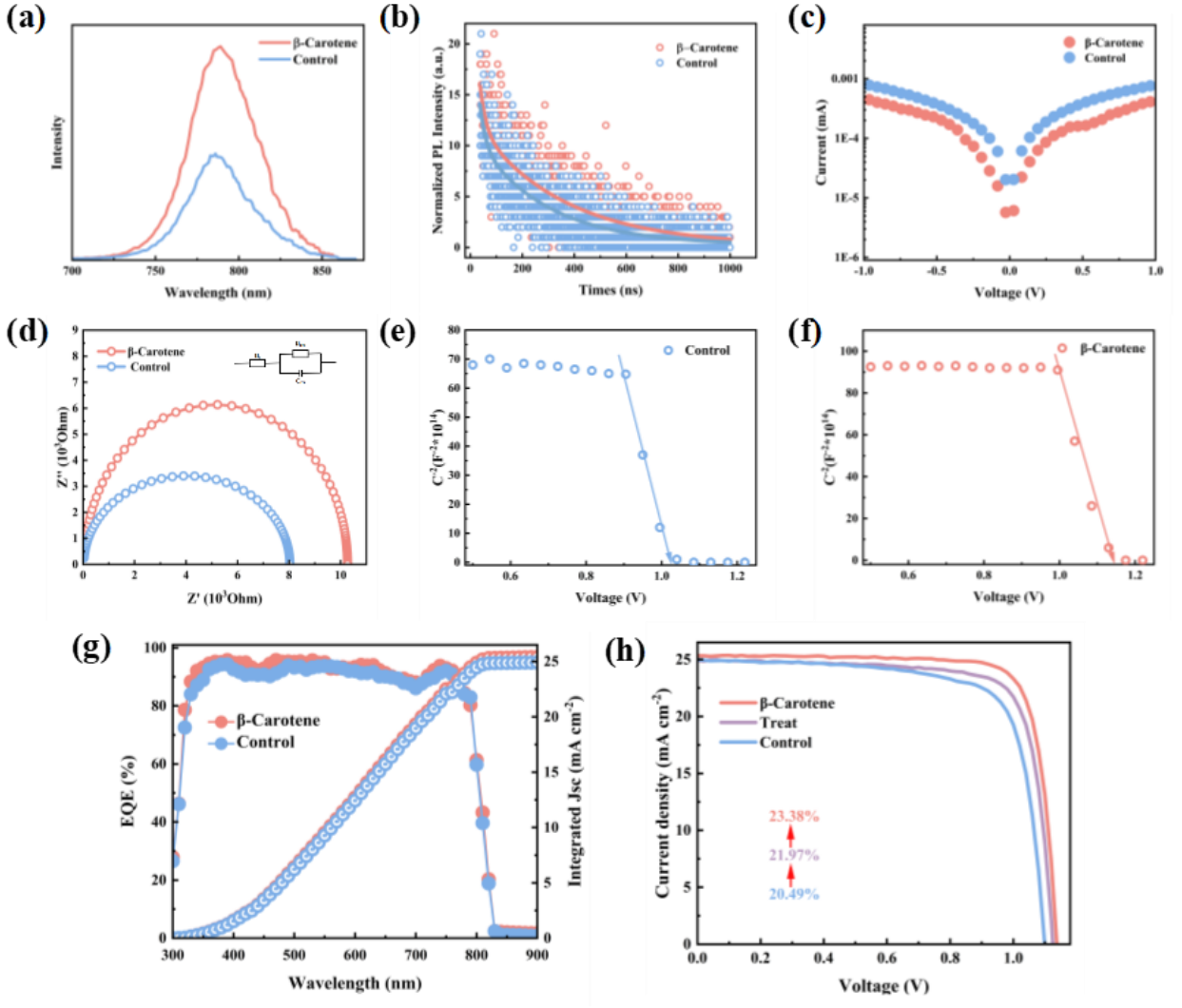

Fig. 4: (a) PL and (b) TRPL test diagrams of perovskite films before and after treatment. (c) J-V curve in dark state of perovskite solar cells. (d) Electrochemical impedance test diagram. (e) Control and (f) processed device Motschottky test diagram. (g) EQE curve and fitting Jsc curve of perovskite devices after β-Carotene antisolvent doping. (h) Final efficiency of perovskite solar cell devices.

is advantageous for improving the PCE of perovskite devices. Time-resolved photoluminescence (TRPL) measurements, as shown in Fig. 4b, revealed that the excited carrier lifetime (τ) in the β-Carotene-treated perovskite film increased from 270 to 337 ns. These findings suggest that β-Carotene effectively inhibited grain nucleation, thereby reducing trap density and suppressing non-radiative recombination at the crystal interface. The dark current of the devices treated with β-Carotene, depicted in Fig. 4c, decreased, indicating reduced current loss due to improved charge recombination processes. This enhancement in charge migration efficiency at the interface also mitigates the aging process of perovskite devices. Electrochemical impedance spectroscopy (EIS) analysis in the high-frequency region (0.1 Hz to 1 MHz) further demonstrated that the carrier capture rate within the perovskite thin films decreased after β-Carotene treatment, leading to better carrier mobility,[30,31] as shown in Fig. 4d. Mott-Schottky (M-S) tests indicated that the internal potential of the β-Carotene anti-solvent-treated perovskite film increased from 1.03 to 1.14 V compared to the control device. This suggests a higher flat-band potential and a significantly enhanced driving force for photogenerated carrier separation in the perovskite film, which contributes to an increase in open-circuit voltage (Voc), as illustrated in Figs. 4e and f. The external quantum efficiency (EQE) data before and after processing, presented in Fig. 4g, shows improved test signals in the short-wavelength region, indicating better interface adaptation and enhanced positive-negative (PN) junction performance in the final perovskite devices.[32] Fig. 4h compares the efficiencies of the control device, the device treated with β-Carotene solution on the upper interface of perovskite, and the device treated with β-Carotene antisolvent doping. While post-treatment passivation of the perovskite surface improved Voc, the fill factor remained suboptimal. This indicates that β-Carotene facilitated better energy level alignment between the perovskite layer and the hole transport

layer in formal devices, providing an ideal conductive channel due to CH-π conjugation. However, the overall photoelectric conversion efficiency was limited by fill factor (FF) and current loss. Perovskite devices with β-Carotene antisolvent doping achieved higher Voc. Jsc, and FF performance due to superior crystal quality and reduced interfacial defect states. Consequently, the final photoelectric conversion efficiency of the perovskite solar cell device was significantly enhanced from 20.49% to 23.38%. Specific test data are shown in Table1.

Table 1: Photoelectric conversion efficiency of control group devices and therapeutic devices by surface passivation of β-Carotene and devices by doping β-Carotene in antisolvent respectively.

	V_{OC} (V)	J_{SC} (mA/cm^2)	FF (%)	PCE (%)
Control	1.10	24.98	74.58	20.49
Treat	1.12	24.93	78.69	21.96
β-Carotene	1.14	25.33	80.99	23.38

Photographs of oxidation were taken for samples containing β-carotene at varying concentrations after being exposed to air for 3 hours following incision. Carrots with the highest concentration of β-carotene exhibited minimal signs of oxidation. Conversely, sections of apples and bananas, which contain lower levels of β-carotene, showed significant blackening after 3 hours. The XRD results depicted in Fig. 5a, obtained after the prepared perovskite film was exposed to an ambient environment for 240 hours, demonstrated that β-carotene provided excellent stability to the perovskite layer. As shown in Fig. 5b, the XRD analysis indicated that the diffraction intensity of the (100) crystal plane of perovskite protected by β-carotene did not significantly decrease, whereas the diffraction peak of perovskite grains in the control group collapsed, leading to a substantial amount of lead iodide precipitation on the surface of the grains (gray-marked area). In tricationic perovskites primarily composed of $FAPbI_3$, the longer Pb-I bond distance of the (100) crystal plane results inenhanced water adhesion (as reported in literature). Consequently, this crystal face, which is advantageous for photoelectric conversion efficiency, is prone to transitioning from the α-$FAPbI_3$ black phase to the δ-$FAPbI_3$ yellow phase due to moisture exposure. Additionally, water intrusion into the perovskite lattice leads to structural degradation, and the

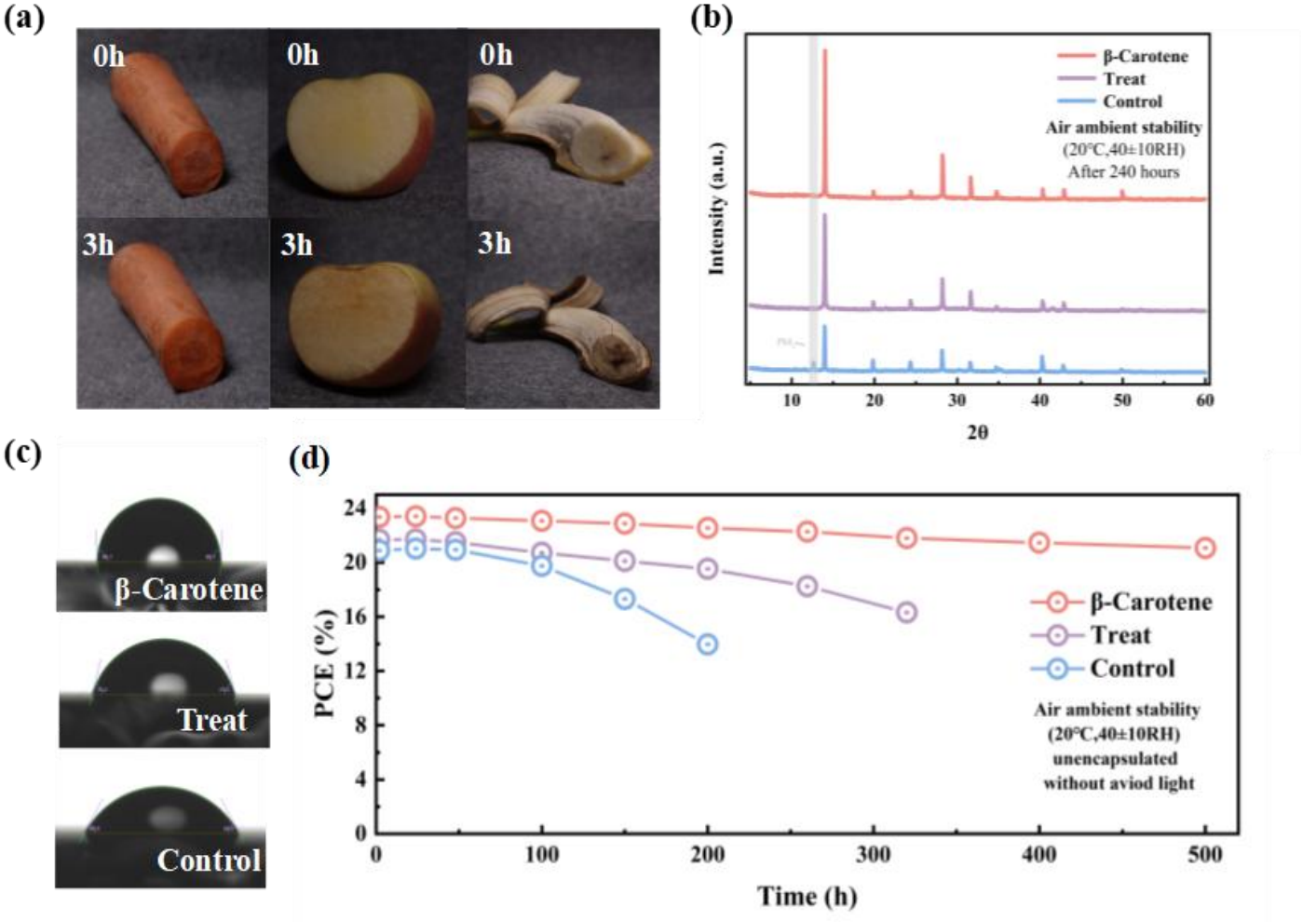

Fig. 5: (a) Sectional oxidation map of articles with different β-Carotene content. (b) XRD test of perovskite crystal stability. (c) Water contact Angle test diagram. (d) Stability test diagram of photoelectric conversion efficiency of perovskite devices.

precipitated lead iodide further accelerates the decline in device stability. The water contact angle test more directly illustrated that β-carotene, as a hydrophobic macromolecular chain, can enhance the moisture resistance of the perovskite crystal structure. As shown in Fig. 5c, uniform-sized water droplets were placed at the same height, and after waiting for 3 seconds, the contact angle between the water droplet and the upper interface of the perovskite was captured. The hydrophobicity of the perovskite surface, after β-carotene surface passivation treatment and β-carotene anti-solvent doping treatment, was significantly improved. Compared to the control device, the water contact angle increased from 60.9° to 75.2° and 90.7°, respectively. β-carotene is inherently hydrophobic due to its conjugated double bonds and lack of polar functional groups. Finally, we evaluated the stability of the photoelectric conversion efficiency of the final device, as shown in Fig. 5d. After 200 hours, the photoelectric conversion efficiency of the control device had dropped to 67% of its initial value, and most devices had completely failed. In contrast, after 500 hours of air exposure, perovskite devices treated with β-carotene anti-solvent doping maintained an impressive photoelectric conversion efficiency exceeding 90%.

4. Conclusion

In summary, the antisolvent-assisted incorporation of β-carotene macromolecular chains serves as an effective defect-passivation strategy, simultaneously repairing intrinsic crystal imperfections and optimizing energy level alignment in perovskite films, ultimately leading to enhanced PCE. The introduction of long alkyl chains effectively mitigates the rapid nucleation of perovskite grains, resulting in larger and better-oriented grains post-annealing. Density functional theory (DFT) calculations reveal that β-carotene's conjugated polyene backbone facilitates interfacial dipole formation, optimizing energy level alignment between the perovskite absorber and Spiro-OMeTAD hole-transport layer. The van der Waals forces and hydrogen bonding between the perovskite thin film and β-carotene are key factors promoting the compact growth of perovskite grains and reducing internal defect states. The hydrophobic organic matter naturally attached to grain boundaries and interfaces significantly enhances the overall hydrophobicity of the device, leading to superior environmental stability. We observed that adding a small amount of β-carotene molecules to the antisolvent further increased the final power conversion efficiency of the perovskite solar cell from 20.49% to an impressive 23.38%. Importantly, our stability tests revealed that the device exhibits excellent stability in humid air environments, maintaining over 90% of its initial efficiency after 500 hours. Our findings demonstrate that the strategic incorporation of natural pigment molecules in perovskite semiconductors effectively stabilizes the crystalline lattice while passivating intrinsic bulk defects, offering a promising materials engineering approach for improved optoelectronic performance.

Acknowledgments

The authors acknowledge financial from the National Natural Science Foundation of China (62304070).

Conflict of Interest

There is no conflict of interest.

Supporting Information

Applicable.

References

[1] H. J. Snaith, Present status and future prospects of perovskite photovoltaics, *Nature Materials*, 2018, **17**, 372-376, doi: 10.1038/s41563-018-0071-z.

[2] E. Aydin, T. G. Allen, M. De Bastiani, A. Razzaq, L. Xu, E. Ugur, J. Liu, S. De Wolf, Pathways toward commercial perovskite/silicon tandem photovoltaics, *Science*, 2024, **383**, eadh3849, doi: 10.1126/science.adh3849.

[3] X. Li, J. Tang, P. Zhang, S. Li, Strategies for achieving high efficiency and stability in carbon-based all-inorganic perovskite solar cells, *Cell Reports Physical Science*, 2024, **5**, 101842, doi: 10.1016/j.xcrp.2024.101842.

[4] M. A. Green, E. D. Dunlop, M. Yoshita, N. Kopidakis, K. Bothe, G. Siefer, D. Hinken, M. Rauer, J. Hohl-Ebinger, X. Hao, Solar cell efficiency tables (version 64), *Progress in Photovoltaics*: *Research and Applications*, 2024, **32**, 425-441, doi: 10.1002/pip.3831.

[5] Z. Xu, X. Zhou, X. Li, P. Zhang, Polymer-regulated SnO_2 composites electron transport layer for high-efficiency n–i–p perovskite solar cells, *Solar RRL*, 2022, **6**, 2200092, doi: 10.1002/solr.202200092.

[6] T. A. Chowdhury, M. A. Bin Zafar, M. Sajjad-Ul Islam, M. Shahinuzzaman, M. A. Islam, M. U. Khandaker, Stability of perovskite solar cells: issues and prospects, *RSC Advances*, 2023, **13**, 1787-1810, doi: 10.1039/D2RA05903G.

[7] E. Aydin, E. Ugur, B. K. Yildirim, T. G. Allen, P. Dally, A. Razzaq, F. Cao, L. Xu, B. Vishal, A. Yazmaciyan, A. A. Said, S. Zhumagali, R. Azmi, M. Babics, A. Fell, C. Xiao, S. De Wolf, Enhanced optoelectronic coupling for perovskite/silicon tandem solar cells, *Nature*, 2023, **623**, 732-738, doi: 10.1038/s41586-023-06667-4.

[8] H. Meng, X. Li, Y. Mai, P. Zhang, S. Li, Enhanced efficiency and stability of triple-cation perovskite solar cells through engineering of the cell interface with phenylethylammonium thiocyanate, *ACS Applied Materials & Interfaces*, 2024, **16**, 69430-69438, doi: 10.1021/acsami.4c16338.

[9] S. Heo, G. Seo, Y. Lee, M. Seol, S. H. Kim, D. J. Yun, Y. Kim, K. Kim, J. Lee, J. Lee, W. S. Jeon, J. K. Shin, J. Park, D. Lee, M. K. Nazeeruddin, Origins of high performance and degradation in the mixed perovskite solar cells, *Advanced Materials*, 2019, **31**, e1805438, doi: 10.1002/adma.201805438.

[10] J. Huang, S. Tan, P. D. Lund, H. Zhou, Impact of H_2O on organic–inorganic hybrid perovskite solar cells, *Energy & Environmental Science*, 2017, **10**, 2284-2311, doi: 10.1039/C7EE01674C.

[11] C. Das, M. Kot, T. Hellmann, C. Wittich, E. Mankel, I. Zimmermann, D. Schmeisser, M. Khaja Nazeeruddin, W. Jaegermann, Atomic layer-deposited aluminum oxide hinders iodide migration and stabilizes perovskite solar cells, *Cell Reports Physical Science*, 2020, **1**, 100112, doi: 10.1016/j.xcrp.2020.100112.
[12] J. Xing, Q. Wang, Q. Dong, Y. Yuan, Y. Fang, J. Huang, Ultrafast ion migration in hybrid perovskite polycrystalline thin films under light and suppression in single crystals, *Physical Chemistry Chemical Physics*, 2016, **18**, 30484-30490, doi: 10.1039/C6CP06496E.
[13] Y. Zhao, I. Yavuz, M. Wang, M. H. Weber, M. Xu, J.-H. Lee, S. Tan, T. Huang, D. Meng, R. Wang, J. Xue, S.-J. Lee, S.-H. Bae, A. Zhang, S.-G. Choi, Y. Yin, J. Liu, T.-H. Han, Y. Shi, H. Ma, W. Yang, Q. Xing, Y. Zhou, P. Shi, S. Wang, E. Zhang, J. Bian, X. Pan, N.-G. Park, J.-W. Lee, Y. Yang, Suppressing ion migration in metal halide perovskite *via* interstitial doping with a trace amount of multivalent cations, *Nature Materials*, 2022, **21**, 1396-1402, doi: 10.1038/s41563-022-01390-3.
[14] S. Huang, Z. Rui, D. Chi, D. Bao, Influence of defect states on the performances of planar tin halide perovskite solar cells, *Journal of Semiconductors*, 2019, **40**, 032201, doi: 10.1088/1674-4926/40/3/032201.
[15] F. Wang, S. Bai, W. Tress, A. Hagfeldt, F. Gao, Defects engineering for high-performance perovskite solar cells, *NPJ Flexible Electronics*, 2018, **2**, 22, doi: 10.1038/s41528-018-0035-z.
[16] J. Jia, J. Dong, B. Shi, J. Wu, Y. Wu, B. Cao, Postpassivation of $Cs_{0.05}(FA_{0.83}MA_{0.17})_{0.95}Pb(I_{0.83}Br_{0.17})_3$ perovskite films with tris(pentafluorophenyl)borane, *ACS Applied Materials & Interfaces*, 2021, **13**, 2472-2482, doi: 10.1021/acsami.0c16939.
[17] X. Zeng, Q. Luo, J. Li, Y. Li, W. Wang, Y. Li, R. Wu, D. Pan, G. Song, J. Li, Z. Guo, N. Wang, A multifunctional pentlandite counter electrode toward efficient and stable sensitized solar cells, *Advanced Composites and Hybrid Materials*, 2021, **4**, 392-400, doi: 10.1007/s42114-021-00233-0.
[18] Y. Zhou, Y.-H. Jia, H.-H. Fang, M. A. Loi, F.-Y. Xie, L. Gong, M.-C. Qin, X.-H. Lu, C.-P. Wong, N. Zhao, Composition-tuned wide bandgap perovskites: from grain engineering to stability and performance improvement, *Advanced Functional Materials*, 2018, **28**, 1803130, doi: 10.1002/adfm.201803130.
[19] L. Zhu, X. Zhang, M. Li, X. Shang, K. Lei, B. Zhang, C. Chen, S. Zheng, H. Song, J. Chen, Trap state passivation by rational ligand molecule engineering toward efficient and stable perovskite solar cells exceeding 23% efficiency, *Advanced Energy Materials*, 2021, **11**, 2100529, doi: 10.1002/aenm.202100529.
[20] K. Fan, Y. Dai, J. Wang, R. Wang, Z. Lu, Y. Lou, G. Zou, Enhanced mechanical stability of perovskite film by modulating the toughness of grain boundary, *Organic Electronics*, 2023, **117**, 106778, doi: 10.1016/j.orgel.2023.106778.
[21] A. M. Naji, S. H. Kareem, A. H. Faris, M. K. A. Mohammed, Polyaniline polymer-modified ZnO electron transport material for high-performance planar perovskite solar cells, *Ceramics International*, 2021, **47**, 33390-33397, doi: 10.1016/j.ceramint.2021.08.244.
[22] F. Bisconti, M. Leoncini, S. Gambino, N. Vanni, S. Carallo, F. Russo, V. Armenise, A. Listorti, S. Colella, S. Valastro, A. Alberti, G. Mannino, A. Rizzo, Mimicking natural antioxidant systems for improved photostability in wide-band-gap perovskite solar cells, *ACS Nano*, 2024, **18**, 1573-1581, doi: 10.1021/acsnano.3c09437.
[23] Z. Qiu, X. Chen, T. Geng, Z. Wan, Q. Lu, L. Li, K. Zhu, X. Zhang, Y. Liu, X. Lin, L. Chen, Z. Shan, L. Liu, A. Pan, G. Liu, Associations of serum carotenoids with risk of cardiovascular mortality among individuals with type 2 diabetes: results from NHANES, *Diabetes Care*, 2022, **45**, 1453-1461, doi: 10.2337/dc21-2371.
[24] J. Terao, Revisiting carotenoids as dietary antioxidants for human health and disease prevention, *Food & Function*, 2023, **14**, 7799-7824, doi: 10.1039/d3fo02330c.
[25] C. Yi, J. Luo, S. Meloni, A. Boziki, N. Ashari-Astani, C. Grätzel, S. M. Zakeeruddin, U. Röthlisberger, M. Grätzel, Entropic stabilization of mixed A-cation ABX_3 metal halide perovskites for high performance perovskite solar cells, *Energy & Environmental Science*, 2016, **9**, 656-662, doi: 10.1039/C5EE03255E.
[26] K. Wang, H. Chen, T. Niu, S. Wang, X. Guo, H. Wang, Dopant-free hole transport materials with a long alkyl chain for stable perovskite solar cells, *Nanomaterials*, 2019, **9**, 935, doi: 10.3390/nano9070935.
[27] L. Kong, X. Cao, K. Liang, R. Wang, J. Liu, W. Shi, C. Lu, Ultrathin carbon nitride nanosheets with fast interlayer charge transfer: toward perovskite solar cells, *The Journal of Physical Chemistry C*, 2023, **127**, 13493-13502, doi: 10.1021/acs.jpcc.3c01687.
[28] S. Akin, N. Arora, S. M. Zakeeruddin, M. Grätzel, R. H. Friend, M. I. Dar, New strategies for defect passivation in high-efficiency perovskite solar cells, *Advanced Energy Materials*, 2020, **10**, 1903090, doi: 10.1002/aenm.201903090.
[29] S. Heo, G. Seo, Y. Lee, D. Lee, M. Seol, J. Lee, J.-B. Park, K. Kim, D.-J. Yun, Y. S. Kim, J. K. Shin, T. K. Ahn, M. K. Nazeeruddin, Deep level trapped defect analysis in $CH_3NH_3PbI_3$ perovskite solar cells by deep level transient spectroscopy, *Energy & Environmental Science*, 2017, **10**, 1128-1133, doi: 10.1039/C7EE00303J.
[30] E. von Hauff, D. Klotz, Impedance spectroscopy for perovskite solar cells: characterisation, analysis, and diagnosis, *Journal of Materials Chemistry C*, 2022, **10**, 742-761, doi: 10.1039/D1TC04727B.
[31] E. Ghahremanirad, O. Almora, S. Suresh, A. A. Drew, T. H. Chowdhury, A. R. Uhl, Beyond protocols: understanding the electrical behavior of perovskite solar cells by impedance spectroscopy, *Advanced Energy Materials*, 2023, **13**, 2204370, doi: 10.1002/aenm.202204370.
[32] Z. Liu, W. Qiu, X. Peng, G. Sun, X. Liu, D. Liu, Z. Li, F. He, C. Shen, Q. Gu, F. Ma, H.-L. Yip, L. Hou, Z. Qi, S.-J. Su, Perovskite light-emitting diodes with EQE exceeding 28% through a synergetic dual-additive strategy for defect passivation and nanostructure regulation, *Advanced Materials*, 2021, **33**,

e2103268, doi: 10.1002/adma.202103268.